Size-dependent filling effect of crystalline celluloses in structural engineering of composite oleogels

Bhattarai, Mamata

2022-04-15

Bhattarai , M , Penttilä , P , Barba , L , Macias-Rodriguez , B , Hietala , S , Mikkonen , K S & Valoppi , F 2022 , ' Size-dependent filling effect of crystalline celluloses in structural engineering of composite oleogels ' , LWT-Food Science and Technology , vol. 160 , 113331 . https://doi.org/10.1016/j.lwt.2022.113331

http://hdl.handle.net/10138/341596
https://doi.org/10.1016/j.lwt.2022.113331

LWT - Food Science and Technology 160 (2022) 113331

Contents lists available at ScienceDirect

LWT

journal homepage: www.elsevier.com/locate/lwt

Size-dependent filling effect of crystalline celluloses in structural engineering of composite oleogels

Mamata Bhattarai [a,1], Paavo Penttilä [b], Luisa Barba [c], Braulio Macias-Rodriguez [d], Sami Hietala [e], Kirsi S. Mikkonen [a,f], Fabio Valoppi [a,f,*]

[a] Department of Food and Nutrition, University of Helsinki, Agnes Sjöbergin Katu 2, P.O. Box 66, 00014, Helsinki, Finland
[b] Department of Bioproducts and Biosystems, Aalto University, P.O. Box 16300, FI-00076, Espoo, Finland
[c] Istituto di Cristallografia, Consiglio Nazionale Delle Ricerche, 34100, Trieste, Italy
[d] Institute of Physics, University of Amsterdam, Science Park 904, Amsterdam, the Netherlands
[e] Department of Chemistry, University of Helsinki, P.O. Box 55, 00014, Helsinki, Finland
[f] Faculty of Agriculture and Forestry, Helsinki Institute of Sustainability Science, University of Helsinki, 00014, Helsinki, Finland

ARTICLE INFO

Keywords:
Oleogels
Fillers
Cellulose
Rheology
X-ray scattering and diffraction

ABSTRACT

Oleogels are a class of solid-fat mimetics that contain a large fraction of oil. Most of these materials have low stiffness and poor oil-binding capacity at commercially viable concentrations, which limits their application in the food and cosmetic industries. To improve their mechanical behavior, we exploited the concepts of particulate-filled materials by developing oil-continuous monoglyceride composites reinforced with crystalline cellulose of various sizes. Cellulose was used as the reinforcing filler material due to its strength, biodegradability, and abundance. The composites gradually stiffened and became more brittle with a progressive increase of the cellulose weight fraction as the maximum packing fraction of fillers approached. This was manifested as an increase in the viscoelastic moduli and yield stress, consistent with the size of the filler. Based on differential scanning calorimetry, X-ray diffraction, X-ray scattering analyses, and microscopic analyses, the inert surface of crystalline celluloses provided a solid substrate for the crystallization of monoglycerides, favoring the lamellar stacking of monoglyceride molecules during the composite oleogel formation regardless of the cellulose size. The present study suggests that cellulose is a suitable bio-based filler material to obtain mechanically strong oleogels suitable for high-shear applications *e.g.,* in food and pharmaceutical industries.

1. Introduction

Oleogels, also known as edible organogels, are structured lipid-based materials that have attracted the attention of academia and industry in the last two decades. Oleogels are anhydrous semi-solid materials with more than 85% oil physically entrapped in either a crystalline network formed by low molecular weight compounds (such as monoglycerides, fatty acids, fatty alcohols, waxes) (Marangoni, van Duynhoven, Acevedo, Nicholson, & Patel, 2020) or a polymeric/particle network formed by crystalline, semi-crystalline polymers, and fibers (Patel, 2018). Materials that have been studied in the latter category are chitin, chitin nanocrystals, ethylcellulose, methylcellulose, hydroxyproplymethylcellulose, cellulose fibers, and protein aggregates (David et al., 2021; de Vries, Hendriks, van der Linden, & Scholten, 2015; Gravelle, Blach, Weiss, Barbut, & Marangoni, 2017; Nikiforidis & Scholten, 2015; Patel et al., 2014; Tanti, Barbut, & Marangoni, 2016). Oleogels are usually prepared by directly mixing the gelators with oil at an elevated temperature for dissolution followed by cooling for crystallization. Oleogels have also been prepared using indirect methods, such as polymer/protein-based emulsions, hydrogels, foams, aerogels through drying, solvent exchange, and/or oil absorption (Patel, 2018).

Structured lipids are potential substitutes of saturated, hydrogenated, and *trans*-fat in food products that have been linked to cardiovascular diseases, type 2 diabetes, and metabolic syndrome (Jang, Bae, Hwang, Lee, & Lee, 2015; Tanti et al., 2016). Other industrial applications include drug delivery, biosensing, and energy storage material (Dhal et al., 2017; Lin et al., 2014; Sakai, Iijima, & Suzuki, 2018). However, most oleogels have a low tolerance towards shear forces, which results in

* Corresponding author. University of Helsinki, Helsinki, Finland.,
E-mail address: fabio.valoppi@helsinki.fi (F. Valoppi).
[1] Department of Bioproducts and Biosystems, Aalto University, Vuorimiehentie 1, 02150, Espoo, Finland.

https://doi.org/10.1016/j.lwt.2022.113331
Received 18 January 2022; Received in revised form 1 March 2022; Accepted 5 March 2022
Available online 7 March 2022

structural breakup and thereby limits their applications. The mechanical properties and oil-retention ability of oleogels have been improved to some extent through modifications in formulation (*e.g.*, increasing amount or combining gelators) and production process (*e.g.*, cooling rate, application of shear forces, ultrasound, and ultrasonic standing waves) (Blake, Co, & Marangoni, 2014; Blake & Marangoni, 2015a; Giacomozzi, Palla, Carrín, & Martini, 2019; Jana & Martini, 2014; Sharifi, Goli, & Fayaz, 2019; Valoppi et al., 2020). However, oleogels are still not mechanically adequate in applications where large deformation is applied, *e.g.,* in lamination during puff pastry dough production.

A possible solution for increasing the shear tolerance of oleogels resides in the use of particles as fillers to form composite oleogels. Fillers are volume-filling particles that are primarily applied to improve materials' mechanical properties (Fu, Feng, Lauke, & Mai, 2008). Engineering of a novel class of composite materials through self-assembly of particles has generated considerable interest, as clustering of particles and their dynamic interactions with other macromolecular constituents of the matrix allow for the synergism of properties of individual constituents. In this regard, crystalline celluloses have attracted significant interest as functional renewable reinforcing agents in composite material given the natural source, tunable surface chemistry, high strength, and large surface area allowing numerous interfacial interactions (De France, Hoare, & Cranston, 2017). Cellulose particles as fillers have been studied in polymer-based hydrogels, where a hierarchically clustered nanocrystalline cellulose-polymer complex significantly improved their mechanical properties (da Silva & Dreiss, 2016). Considering recent interest to expand the utilization of cellulose-based materials, we developed monoglyceride-based crystalline cellulose-filled composite oleogels. The functionality of fillers in a composite matrix depends on particle size, particle loading, and particle-matrix interface interaction (Fu et al., 2008). To investigate these effects, three cellulose crystals from micro-to nanoscale were used as fillers in a monoglyceride-based oleogel. The effect of progressive addition of crystalline celluloses on the mechanical properties at small- and large-amplitude oscillation strain were studied. To understand the filler-matrix interaction, the micro- and nanostructure of composite oleogels were studied by microscopy, synchrotron X-ray diffraction and small-angle X-ray scattering techniques. Finally, the melting properties and oil-retention ability of composite oleogels were investigated.

2. Materials and methods

2.1. Materials

Dry microcrystalline celluloses, Arbocel M80 (bulk density 0.20–0.24) and Vivapur 105 (bulk density max 0.26), were kindly provided by JRS Pharma Oy (Nastola, Finland). Desulfated cellulose nanocrystals (DS-CNC) slurry was purchased from Cellulose Lab (Fredericton, Canada). The slurry was freeze dried followed by milling for 1 min using a Siebtechnik Tema vibratory mill (Rijswijk, Netherlands) mounting concentric stainless-steel discs. The average particle size of crystalline celluloses decreased in the following order (data provided by the manufacturer): Arbocel (55 μm), Vivapur (15 μm), and DS-CNC (10–20 nm width, 50–400 nm length). All celluloses were dried for 5 days in a vacuum oven at 30–40 °C before use. Myverol 18–04 K saturated monoglyceride (fatty acid composition: 42–48% C16:0, 50–60% C18:0; melting point 68.05 ± 0.5 °C) was donated by Kerry Ingredients and Flavours (Bristol, UK). Rapeseed oil from Raisio was purchased from a local supermarket. Isobutanol was purchased from Merck KGaA (Darmstadt, Germany).

2.2. Oleogel preparation

First, a monoglyceride-containing oleogel was prepared by mixing 5% monoglycerides with rapeseed oil at 80 °C. The molten mixture was blended with crystalline celluloses at increasing weight fractions (0, 2.5, 5, 10, 20, 30, 40, and 50%) using a magnetic stirrer (or spatula if needed) at 80 °C. Samples crystallized by immersing the container in a water bath at 20 °C (10–20 min) and stored at room temperature (RT) overnight before analyses. Dispersions of celluloses were prepared by mixing 40% cellulose in rapeseed oil at RT. All concentrations are expressed as mass percentage (% w/w).

2.3. Rheology

Large amplitude oscillatory shear (LAOS) and small amplitude oscillatory shear (SAOS) measurements were performed in a hybrid rheometer Discovery HR-2 (TA Instruments, Delaware, USA) using 20 mm parallel plate geometry at 22 °C. Sandpaper with an average grit of 600 was glued on both plates to prevent slipping of samples. Samples were carefully placed between the plates with a gap of 3–3.5 mm. Axial force was allowed to stabilize for 2–3 min before the measurement. For the LAOS and SAOS measurements, an oscillation strain 0.001–1000% and 0.001–100% were applied, respectively, with an angular frequency of 2 rad/s. To study the recovery of oleogels, two amplitude sweeps were recorded during SAOS measurements. First, an oscillation strain of 0.001–100% was applied followed by a 5 min rest period, and a second sweep was performed. Measurement data were collected in transient mode by Trios software 5.1 (TA Instruments). Sampling time was 8 cycles sinusoidal waves with 191.75 points per cycle. The yield stress and critical strain were calculated as an intersection point of two linear lines in the stress-strain curve (Dinkgreve, Paredes, Denn, & Bonn, 2016). Analysis of LAOS responses was performed according to Macias-Rodriguez, Ewoldt, and Marangoni (2018).

The recovery ratio (R_r) of oleogel samples was calculated using:

$$R_r = \frac{(G_1^* - G_2^*)}{G_1^*} \quad (1)$$

where, G^*_1 and G^*_2 are the average complex moduli from the first and second amplitude sweeps in the viscoelastic region, respectively.

The recovery ratio as a function of cellulose concentration was fit using a one-phase association model:

$$R_r = R_{r0} + (P - R_{r0}) \cdot \left(1 - e^{-k \cdot C}\right) \quad (2)$$

where R_{r0} is the theoretical recovery ratio of the plain oleogel, (set to 0.6339 as experimentally determined), P is the maximum theoretical recovery ratio at the plateau (in this case equal to 1), k is the rate constant, and C is the cellulose concentration expressed as weight percentage over the total composite oleogel weight.

The complex modulus G^* as a function of cellulose concentration was fit using a Krieger-Dougherty type equation (Krieger & Dougherty, 1959):

$$G^* = G_0^* \cdot \left(1 - \frac{C}{C_{max}}\right)^{-n \cdot C_{max}} \quad (3)$$

where G^*_0 is the complex modulus at 0% cellulose concentration, C_{max} is the maximum mass cellulose concentration (vertical asymptote of the hyperbolic function), and n is a fitting constant. For further analysis, cellulose concentration was divided by a scaling factor arbitrarily chosen to be positively correlated with cellulose particle size and set to Arbocel = 1; Vivapur = 1.08; DS-CNC = 2.7.

Non-linear regression analysis was performed on recovery ratio and G^* as a function of cellulose concentration using TableCurve 2D version 5.01 (Jandel Scientific Software, San Rafael, CA, USA). The Levenberg-Marquardt algorithm was used to perform least-squares function minimization. Goodness of fit was evaluated based on statistical parameters of fitting (R^2, p, standard error) and residual analysis.

2.4. Microscopy

Microstructure of oleogels was analyzed using an Axio Lab A1 polarized light microscope (Zeiss, Oberkochen, Germany) with Axiocam 305 (Zeiss). An aliquot of sample was placed on a glass slide with coverslip gently pressed on top. Images were acquired and processed using ZEN 2.6 (Zeiss).

2.5. Scanning electron microscopy (SEM)

Microstructural analysis of dry cellulose powders and selected oleogels was performed using SEM. Before imaging oleogels were deoiled using isobutanol (Blake & Marangoni, 2015b). Samples were gently transferred onto 25 mm diameter 0.2 μm pore-sized polycarbonate disks (Whatman, Maidstone, UK) placed on top of Whatman 1 filter paper. Isobutanol was added dropwise on the surface of samples and allowed to dry for 48 h at RT before imaging. Samples were coated with Au–Pd alloy (2-nm thick layer) using a Cressington HR208 high-resolution sputter coater (Cressington Scientific Instruments, Watford, UK). Imaging was performed at RT with a Hitachi S-4800 (Hitachi High-Technologies Corporation, Tokyo, Japan) field emission scanning electron microscope.

2.6. Synchrotron light X-ray diffraction (XRD)

X-ray diffraction patterns were recorded at the XRD1 beamline, Elettra Synchrotron Radiation Facility in Trieste, Italy. The X-ray beam emitted by the wiggler source on the Elettra 2 GeV electron storage ring was monochromatized by a Si (111) double crystal monochromator, focused on the sample and collimated by a double set of slits to a spot size of 200 μm × 200 μm. Celluloses were analyzed by lodging the powders into a 0.3-mm diameter glass capillary (WJM-Glas Müller GmbH, Berlin, Germany). Oleogels were analyzed by lodging a sample aliquot into a nylon pre-mounted cryoloop 20 μm for crystallographic experiments (0.7–1.0 mm) (Hampton Research HR4-965, Aliso Veijo, CA, USA). Analyses were performed at approximately 22–23 °C. Data were collected at a photon energy of 8.856 keV ($\lambda = 1.4$ Å) using a 2 M Pilatus silicon pixel X-ray detector (DECTRIS Ltd., Baden, Switzerland). Bidimensional patterns collected with Pilatus were calibrated using lanthanum hexaboride powder (LaB_6, standard reference material 660a of NIST) and integrated using FIT2D software version 12.77 (Hammersley, Svensson, Hanfland, Fitch, & Hausermann, 1996) obtaining a pattern of diffracted intensity *vs* diffraction angle for every sample. The 2θ range spanned from 1° to 30° and the resolution reached 2.6 Å. Profile fitting of the X-ray diffraction peaks obtained by the crystalline phase was performed using WinPlotr version July 2017 (Roisnel & Rodríguez-Carvajal, 2000). In most cases, a collective value of full width at half maximum (FWHM) of 0.02° was assumed to refine their position along with a Lorentzian model for the amorphous contribution to the background. Peak positions and intensity plots are represented as a function of scattering vector (q) corresponding to 2θ as following:

$$q = \frac{4\pi \cdot \sin\theta}{\lambda} \tag{4}$$

The thickness of the crystal L (perpendicular to the lamella) was estimated using the Scherrer equation:

$$L = \frac{\lambda}{\beta \cdot \cos\theta} \tag{5}$$

where β is the integral breadth defined as the ratio of peak area (of the peak recorded in the small-angle region) to peak height. In this case, β was used to characterize the peak broadening and a shape factor of 1 was used instead of commonly used FWHM and shape factor of 0.9 for lipid crystalline domain size calculation (Acevedo & Marangoni, 2010). The Scherrer equation assumes that the crystalline shape is cubic, therefore β and a shape factor of 1 can be used for the 100 reflection from cubic crystals (Langford & Wilson, 1978).

2.7. Small angle X-ray scattering (SAXS)

Nanostructural analysis of selected samples was performed using SAXS technique. A Xenocs Xeuss 3.0 C (Xenocs, Sassenage, France) SAXS device including a GeniX 3D Cu microfocus source and EIGER2 R 1M hybrid pixel detector was used. The sample to detector distance was 1.1 m and the X-ray wavelength was $\lambda = 1.542$ Å. Measurements were performed on pure rapeseed oil, Vivapur dispersed in oil at 1% and 30%, 5% monoglyceride oleogel, and composite oleogels with 5% and 30% Vivapur. Samples were carefully placed in a 0.5- or 1-mm thick gel cells with Kapton window. The measured intensities were corrected for cosmic radiation in the instrument software, integrated azimuthally over a full circle, divided by transmitted beam intensity, and normalized to an absolute scale using a glassy carbon sample. The scattering from an empty cell was subtracted and the intensities were scaled by dividing with sample cell thickness.

First, the scattering contribution from oil in all oleogel samples and cellulose dispersions was subtracted by considering the volume displaced by the components (Pauw, Smith, Snow, Terrill, & Thünemann, 2017). The volume fractions were calculated using the density value of 0.9 g/cm^3 for oil and monoglycerides and 1.5 g/cm^3 for Vivapur. The oil-subtracted oleogels were further subtracted with scattering contributions from the cellulose and monoglycerides to elucidate the structure of monoglycerides and cellulose in the composite oleogels, respectively (Fig. S2, supporting information). During these subtractions, numerical factors were adjusted manually.

The diffraction peak was fitted with a pseudo-Voigt function with peak location q_{max} and integral breadth β, and a linear background (Fig. S3, supporting information). The lattice spacing (lamellar periodicity) was determined as $d_{001} = 2\pi/q_{max}$, and the thickness of crystal L was estimated using the Scherrer equation in q-space $L = 2\pi/\beta$. This analysis assumes that the peak broadening is only caused by the limited crystal size. To consider any variation of the lattice spacing, data was further fitted using an analytical model corresponding to a stack of repeating lamellar structures where the lamellar spacing has a Gaussian distribution (Bergström, Pedersen, Schurtenberger, & Egelhaaf, 1999). The number of stacked bilayers and the polydispersity of lattice spacing (relative standard deviation of the Gaussian distribution) was calculated using the "lamellar stack paracrystal" model in SasView 5.0.3 software (Doucet et al., 2020) with the sheet thickness parameter fixed to 15 Å. The thickness parameter reflects the thickness of headgroups of stacked monoglyceride molecules in the crystalline structure.

2.8. Differential scanning calorimetry

Thermal properties of oleogels were analyzed using a DSC823^e differential scanning calorimeter (Mettler Toledo, Columbus, USA) mounted with a TSO801RO sample robot (Mettler Toledo). Samples were prepared by carefully weighing 6–9 mg in 40-μL aluminum DSC pans. Samples were kept at 20 °C for 10 min and heated from 20 to 80 °C at 5 °C/min. Measurements were performed under nitrogen flow (50 mL/min). The peak melting temperature was taken as the minimum value of heat flow during transition. Total peak enthalpy (ΔH) was calculated by integrating melting curves. Data were processed using STAR^e DB V9.00 software (Mettler Toledo).

2.9. Accelerated oil release test

Approximately 1.2 mL of molten sample was poured into 1.5 mL microtubes (Eppendorf, Hamburg, Germany) and cooled in a water bath at 20 °C for 10 min. After overnight storage at RT, samples were centrifuged at 27 464 g for 30 min in a temperature-controlled SL 8R centrifuge (Thermo Scientific, Osterode am Harz, Germany) at 20 °C.

Centrifugal forces applied in this work are higher than those used in the literature for oleogel oil release tests (Blake & Marangoni, 2015a; Valoppi, Calligaris, & Marangoni, 2017), to properly differentiate between samples. Immediately afterward, microtubes were inverted and oil was drained for 5 min. The released oil was calculated as a percentage ratio between the mass of released oil over the total mass of oil in the oleogel.

2.10. Data analysis

All determinations were expressed as mean ± standard deviation of at least two measurements from two experimental replicates ($n \geq 2 \times 2$) if not otherwise specified. Statistical analysis was performed using R software version 3.5.1. Bartlett's test was used to assess the homogeneity of variance. One-way ANOVA was performed, and Tukey's test was used as a post-hoc test to determine significant differences among means ($p < 0.05$).

3. Results and discussion

3.1. Macro-, micro-, and nanostructures of oleogels

The monoglyceride-based oleogel appeared as a soft, semi-solid, spreadable lipid material (Fig. 1, plain oleogel). Upon adding cellulose particles, composite oleogels with seemingly higher opacity were obtained, as assessed visually. Progressive addition of cellulose turned the oleogel into a moldable material (20%–40% Arbocel or Vivapur, or 30%–50% DS-CNC) and eventually into a brittle one (50% Arbocel or Vivapur) (Fig. 1). This indicated that the size and concentration of filler affected the overall structure of oleogels. As a result, microcrystalline celluloses, Arbocel, and Vivapur exhibited better structuring abilities at low concentrations than DS-CNC. The composite oleogel obtained with the largest and smallest-sized celluloses (Arbocel at 40% concentration and DS-CNC from 10% concentration onwards) were grainy, whereas composite oleogels containing Vivapur at all studied concentrations appeared smooth. Even 40% cellulose could not produce a stable gel without monoglycerides. The dispersion of cellulose and oil separated with time (data not shown) indicated the synergistic effect of monoglycerides and cellulose in the oil structuring. Our observation contrasted with the recently reported single-component oil structuration by cellulose fibers (David et al., 2021), where stable oleogels were obtained at fibers concentration of 30%. The dimensions of our cellulose micro- and nanocrystals were smaller compared to the fibers used by David et al. (2021) and therefore did not form an entangled network able to structure oil.

Microscopic analyses were performed to understand the effect of cellulose particles on oleogel microstructure. Fig. 2 shows polarized light micrographs of plain oleogel, micro- and nanocrystalline celluloses dispersed in oil, and composite oleogels with increasing weight fractions of Arbocel, Vivapur, and DS-CNC. Arbocel and Vivapur in oil appeared as elongated fibers with the first one being longer than the second one. On the other hand, DS-CNC in oil appeared as spherical aggregates; most of them were smaller compared to Arbocel and Vivapur. Thus, the total interfacial area relatively increases in the order of Arbocel, Vivapur, and DS-CNC. Plain oleogel was composed of platelet-like interconnected microcrystals of monoglycerides with dimensions between 10 and 50 μm, consistent with previous results (Giacomozzi et al., 2019; Lopez--Martinez et al., 2014; Valoppi, Calligaris, Barba, et al., 2017). When celluloses were added to oleogels at any concentration, the morphology of monoglyceride crystals changed from platelet-like structure to

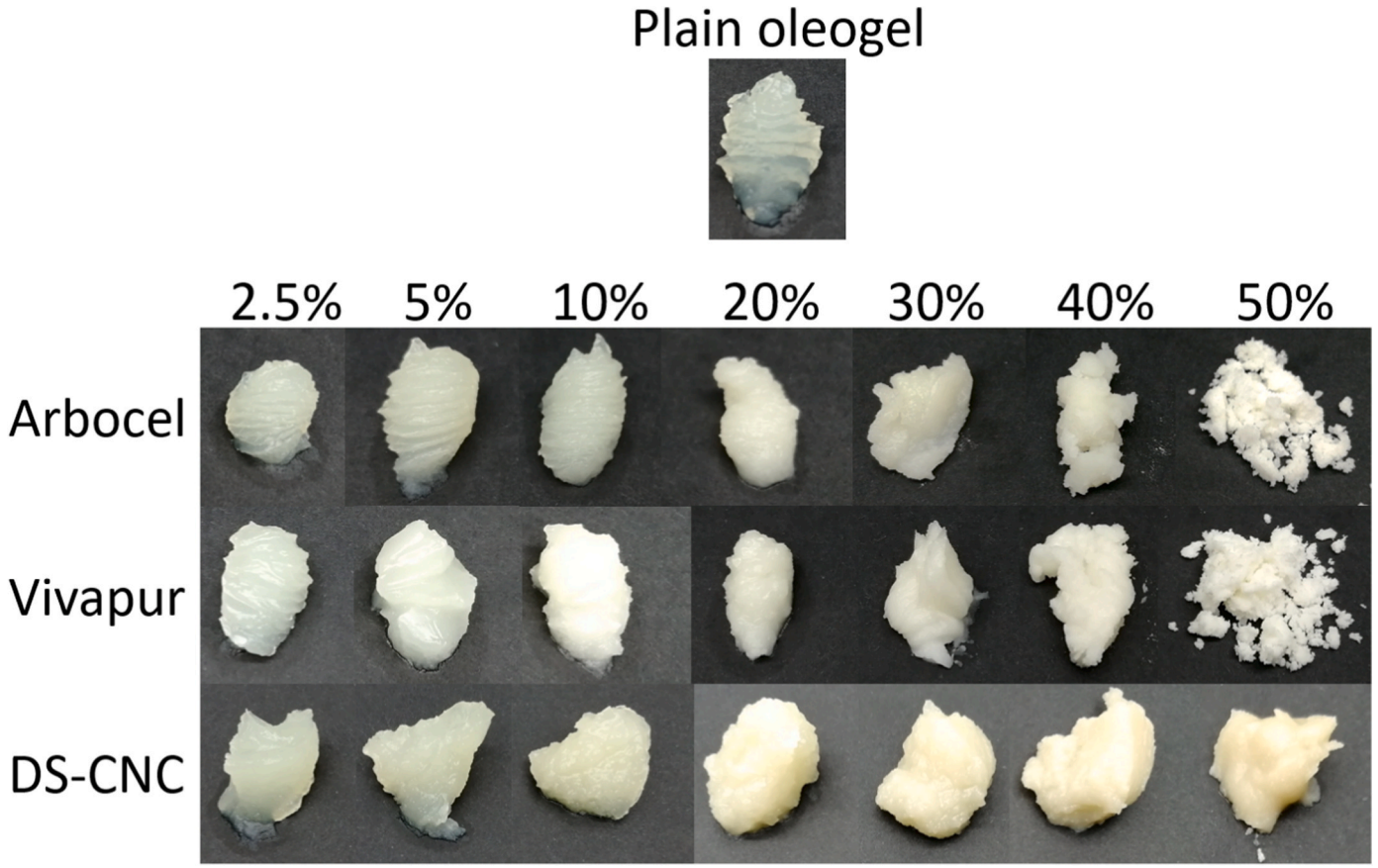

Fig. 1. Visual appearance of oleogels containing increasing concentrations (2.5%, 5%, 10%, 20%, 30%, 40%, and 50%) of cellulose crystals (Arbocel, Vivapur, and DS-CNC). Plain oleogel (0% cellulose) is shown as a reference.

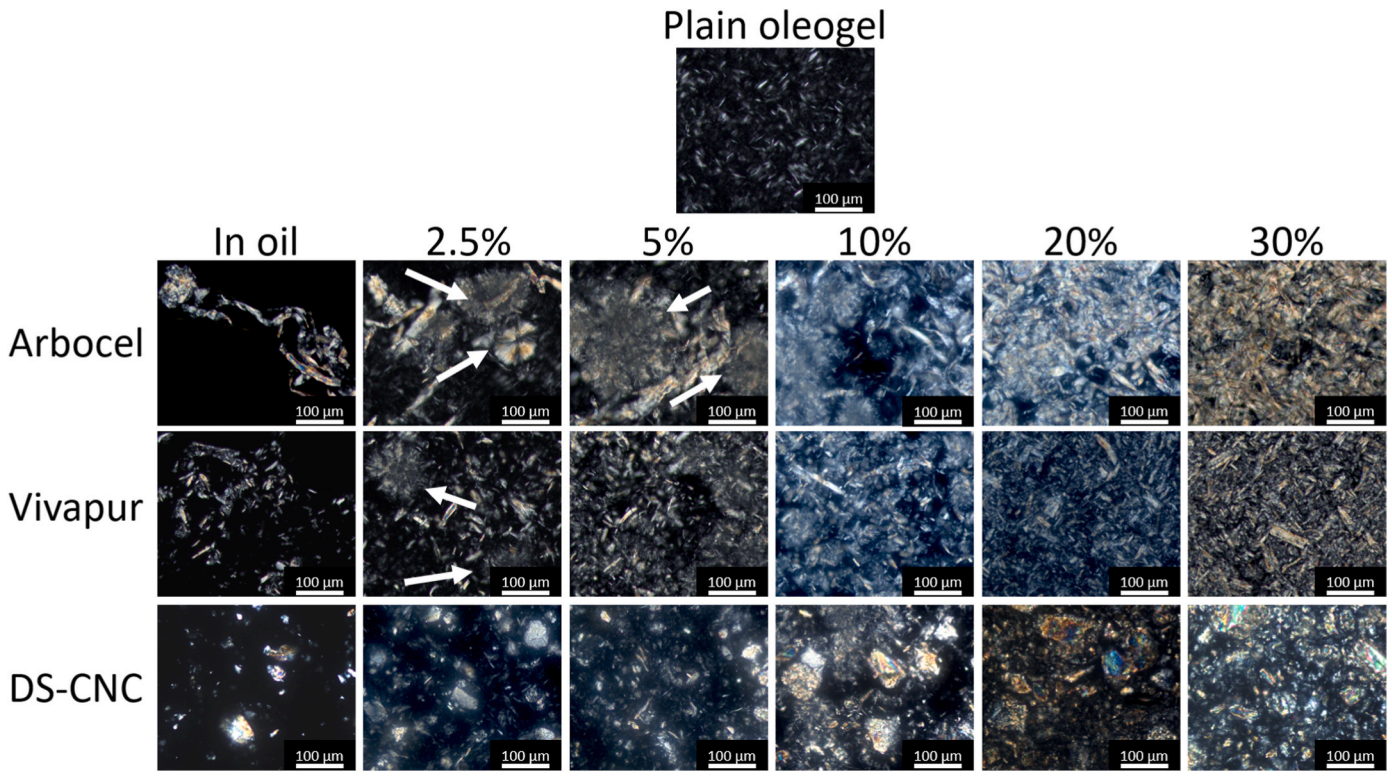

Fig. 2. Microscopic images of composite oleogels containing increasing concentrations (2.5%, 5%, 10%, 20%, and 30%) of cellulose fillers (Arbocel, Vivapur, and DS-CNC). Plain oleogel (0% cellulose) and celluloses dispersed in oil are shown as references. White arrows show the presence of crystalline spherulites.

spherulites with dimensions of 100–200 μm at low cellulose weight fraction (white arrows in Fig. 2). With increasing cellulose content, a progressively jammed microstructure of cellulose and monoglyceride crystals was observed. At the same weight fraction, the jamming was less apparent in oleogel with nanocrystalline cellulose (DS-CNC). An increase of cellulose concentrations to 40% and 50% led to a very dense microstructure (data not shown).

The observed microstructural changes in monoglyceride crystals upon cellulose addition could be attributed to their role as nucleating points during monoglyceride crystallization. The presence of particles or foreign materials are known to modify the morphology of lipid crystals (Yoshikawa, Kida, & Sato, 2015). If foreign materials are wetted by

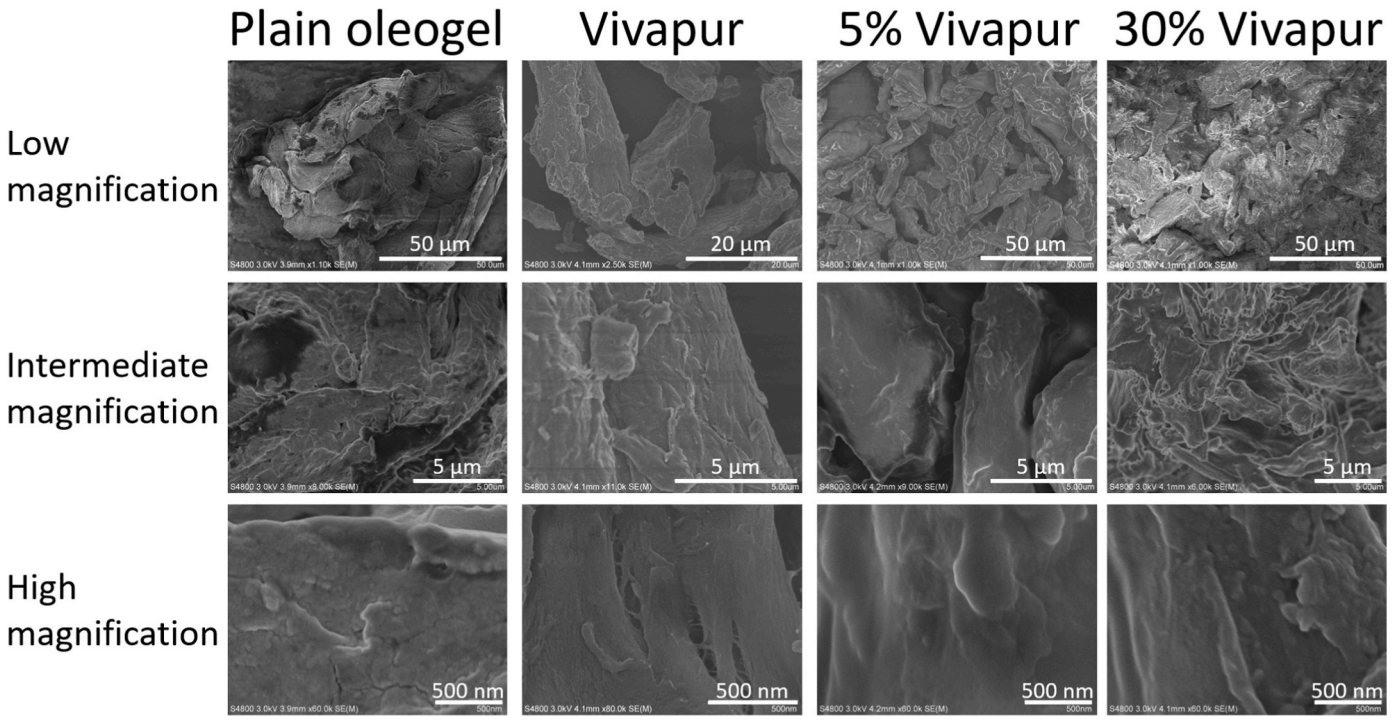

Fig. 3. SEM images of plain oleogel (0% cellulose), Vivapur microcrystalline cellulose powder, and selected composite oleogels containing 5% and 30% Vivapur.

crystallizing molecules, heterogenous nucleation occurs as the energy barrier to form stable nuclei decreases. Due to the affinity between cellulose and monoglycerides (Xiao, Zhang, Zhang, Lu, & Zhang, 2003), crystallization could have initiated from the surface of cellulose micro- and nanocrystals. In SEM images (Fig. 3), surface of cellulose microcrystals appeared irregular while the surfaces of composite oleogels were smooth like observed for the plain oleogel. This suggests the possibility that monoglycerides may have crystallized on the surface of cellulose crystals during the cooling.

The interactions between cellulose and monoglyceride in composite oleogels were investigated in detail by studying the thermal properties and nanostructures by XRD and SAXS analyses.

Based on DSC results, a broad thermal event was observed in all samples (Fig. S1A, supporting information). The melting temperature (taken as transition peak – T_{peak}) of plain oleogel was 58.3 °C, similar to previously reported values (Da Pieve, Calligaris, Panozzo, Arrighetti, & Nicoli, 2011; Giacomozzi et al., 2019). Microcrystalline celluloses slightly increased the melting temperature of composite oleogels. For Arbocel and Vivapur at any weight fraction, it was 59.5 ± 0.5 °C and 59.3 ± 0.5 °C, respectively while for nanocrystalline celluloses DS-CNC the increase was negligible (58.6 ± 0.3 °C). The enthalpy of melting reduced linearly with cellulose concentration due to reduction in the overall concentration of monoglyceride (Fig. S1B, supporting information).

This minimal increase in the melting point of composite oleogels indicate an unchanged polymorphic form of monoglyceride crystals after addition of celluloses. However, microscopic images in Figs. 2 and 3 suggest modification in the crystalline morphology at the micro level. Therefore, XRD and SAXS were employed to investigate whether cellulose addition affected the nanostructural assembly of monoglycerides. Based on XRD results, monoglyceride crystals in plain oleogel organized in triclinic β form (revealed by the peaks between 4.55 and 3.55 Å) with a lamellar structure (d_{001} followed by its higher-order crystallographic reflecting planes belonging to the 00*l* family at the relative peak position of 1/2, 1/3, 1/4) with a thickness of 48.4–48.5 Å (Fig. 4A and B, full list of diffraction peaks reported in Table S1, supporting information). This was in agreement with previously reported studies (Da Pieve, Calligaris, Co, Nicoli, & Marangoni, 2010; Valoppi, Calligaris, Barba, et al., 2017). Addition of cellulose micro- or nanocrystals at 5% or 30% concentration did not affect the polymorphic form and lamellar thickness of monoglyceride crystals in composite oleogels. The crystalline structure of cellulose, characterized by bumps in the 6–3 Å range (full list of diffraction peaks reported in Table S2), was also detected in the XRD patterns of composite oleogels (arrows in Fig. 4B). However, the major impact of cellulose on the nanostructure of monoglyceride in composite oleogels was found in the shape of the main peak recorded at $q = 0.13$ $Å^{-1}$ (48.4 Å). Assuming that the lattice spacing remains constant, the peak shape is directly related to the dimension of crystallite domain (Acevedo & Marangoni, 2010). To obtain more information on the crystallite domain size, we calculated the thickness of the crystal (*L*) using the Scherrer equation for all oleogels shown in Fig. 4. The value of *L* was 497 Å in plain oleogel. The value increased to 600 Å, 589 Å and 501 Å in composite oleogels containing 5% Arbocel, Vivapur and DS-CNC, respectively, and was 602 Å, 796 Å, and 471 Å with 30% cellulose concentration. This indicated that microcrystalline celluloses, Arbocel, and Vivapur increased the thickness of monoglyceride nanocrystals, meaning that the assembly of monoglyceride nanocrystals were promoted. DS-CNC had a negligible effect, illustrating the size-dependent effect of the fillers.

To gain further insight into the nanostructural characteristics of oleogels, SAXS measurements were performed on plain oleogel, selected composite oleogels containing 5% and 30% Vivapur, and Vivapur dispersed in oil at 1% and 30% weight fraction (Fig. 5A and B). Vivapur was selected because of its stronger signals recorded in the diffraction patterns.

All samples exhibited power-law behavior of form $I(q) \propto q^{-\alpha}$. The intensity at low *q* followed a power law with exponent α close to 4. This behavior most likely originated from a smooth interface between oil and either the cellulose crystals or assembled monoglyceride crystals/platelets in the length scale of ≥10 nm (Peyronel, Ilavsky, Pink, & Marangoni, 2014). Composite oleogels also exhibited a second power-law behavior with α close to 3 (Fig. 5B), which can be associated with mass fractal structures of <20 nm (Schmidt, 1991), which likely represent the porous inner structure of cellulose particles. Except for concentration-related differences, SAXS intensities of both composite oleogels were rather similar. Subtracting contributions other than that of oil did not yield any significant additional information at $q < 0.1$ $Å^{-1}$ (Fig. S2, supporting information).

Similarly to XRD results, the SAXS data from oleogels showed the d_{001} diffraction peak from the lamellar monoglyceride crystals at $q = 0.13$ $Å^{-1}$ (48 Å) and became sharper with increasing cellulose amounts in composite oleogels. From the Scherrer equation, the thickness of the crystal (*L*) for plain, 5%, and 30% Vivapur oleogels were calculated as 483 Å, 549 Å, and 671 Å, respectively, in agreement with the trend calculated from XRD data. According to the fits of the analytical model for lamellar stacks (Bergström et al., 1999) (Fig. S4), the number of stacked bilayers of monoglyceride crystals increased from 22 in plain oleogel to 23–26 in composite oleogels. At the same time, the crystal polydispersity of the lamellar spacing d_{001} reduced from 0.084 (plain oleogel) to 0.079 and 0.065 upon the addition of 5% and 30% Vivapur, respectively. Taken together, the SAXS and XRD analyses indicate that microcrystalline cellulose Vivapur enabled the formation of more uniform (narrower Gaussian distribution of d_{001}) and larger crystals (larger number of layers and crystal thickness *L*) of monoglycerides in composite oleogels. This could be explained by the cellulose offering surface area for efficient packing during nucleation and crystal growth forming more regular lamellar stacks.

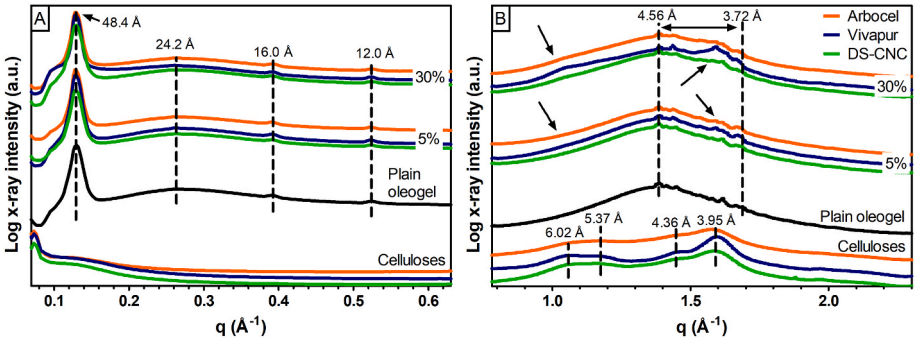

Fig. 4. (A) Small-angle and (B) wide-angle synchrotron X-ray diffraction patterns of plain oleogel (0% cellulose), selected composite oleogels (5% and 30% Arbocel, Vivapur, and DS-CNC), and pure celluloses (Arbocel, Vivapur, and DS-CNC).

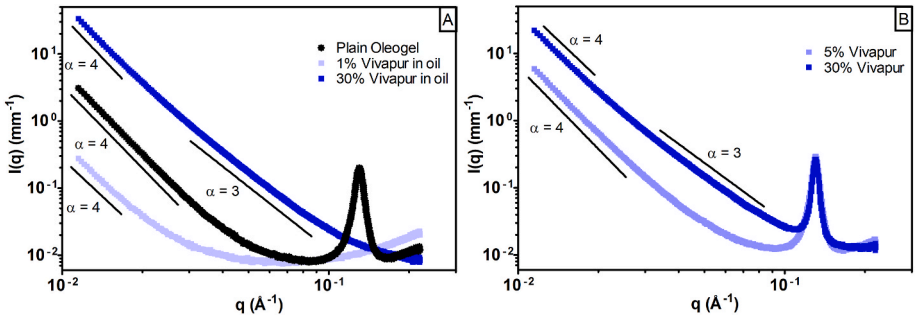

Fig. 5. (A) Small-angle X-ray scattering intensity as a function of scattering vector q of plain oleogel (0% cellulose) and dispersions of 1% and 30% Vivapur in oil after subtracting the scattering from oil. (B) Small-angle X-ray scattering intensity as a function of scattering vector q of composite oleogels containing 5% and 30% Vivapur after subtracting the scattering contributions from oil. Power laws with exponents α = 3 or 4 are plotted for reference.

3.2. Rheological properties and oil-retention ability

The rheological profiles of plain oleogel and composite oleogels from all three celluloses at different concentrations were evaluated. Oleogels displayed gel-like behavior, that is $G' > G''$ for all studied systems (Fig. S5), and a yield stress σ_y, taken as the maximum "peak stress" beyond which flow is induced. The addition of all cellulosic fillers increased the stiffness of the composite oleogels, indicated by increase in the moduli and yield stress from approximately 10^2 to 10^4 Pa to a different degree depending on their weight fraction (Fig. 6). The order of reinforcement was Arbocel > Vivapur > DS-CNC, which is inversely proportional to their relative interfacial areas. As the concentration of the filler increased, the composite oleogels became more brittle as $G^* = \sigma/\gamma$. In most cases, at strain values > 100%, stable flow was not obtained. To explore these effects further, we performed oscillatory tests to measure residual elasticity after inducing flow, herein simplified as a relative "recovery" ratio (Eq. (1) and Eq. (2)) (Fig. 7A) and scaled the complex moduli G^* as a function of weight fraction (Eq. (3)) (Fig. 7B). We observed that celluloses retained the elasticity of oleogels, and the microcrystalline celluloses Arbocel and Vivapur, were better than nanocrystalline cellulose (DS-CNC) at higher weight fraction. This was also observed in the higher rate constant (k) value obtained from fitting of the recovery ratio using a one-phase association model (Fig. 7A, inset table). A possible explanation is that large particles occupy a larger volume and shield the plain oleogel network from damage compared to small particles at the same weight fraction. Scaling the moduli reveals that microcrystalline cellulose is a more effective structurant than nanocrystalline cellulose on a weight-fraction basis (Fig. 7B). This can be visualized in the strong "jump" of the complex moduli and yield stress of microcrystalline-based composites at a concentration of 40%, as the fillers approach the maximum packing fraction of solids.

To elucidate whether fillers gradually affect the yielding response of the composites, we plotted a Lissajous-curves "compositional" space of representative fillers (Fig. 8) and computed local non-linear descriptors of elasticity and viscosity (Fig. S6) as previously applied to fat crystal networks (Macias-Rodriguez et al., 2018). Inspection of the compositional space reveals all samples shared similar mechanical transitions from a linear viscoelastic response (tight ellipses) to a nonlinear viscoelastic (increasingly open ellipses with an upturn). Although the local intracycle response displays local stress stiffening/thickening (stress upturns) (Macias-Rodriguez et al., 2018; Macias-Rodriguez & Marangoni, 2017), the average response remains softening/thinning of the

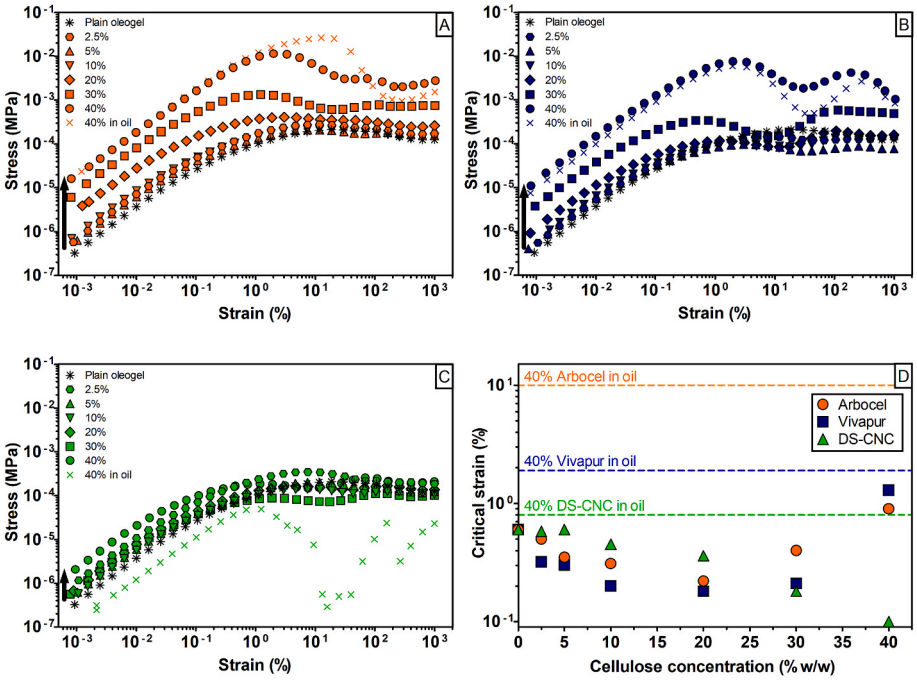

Fig. 6. Stress versus strain curves of oleogels and dispersions containing celluloses (A) Arbocel (B) Vivapur, and (C) DS-CNC. (D) Critical strain as a function of cellulose amount calculated from the stress-strain curve.

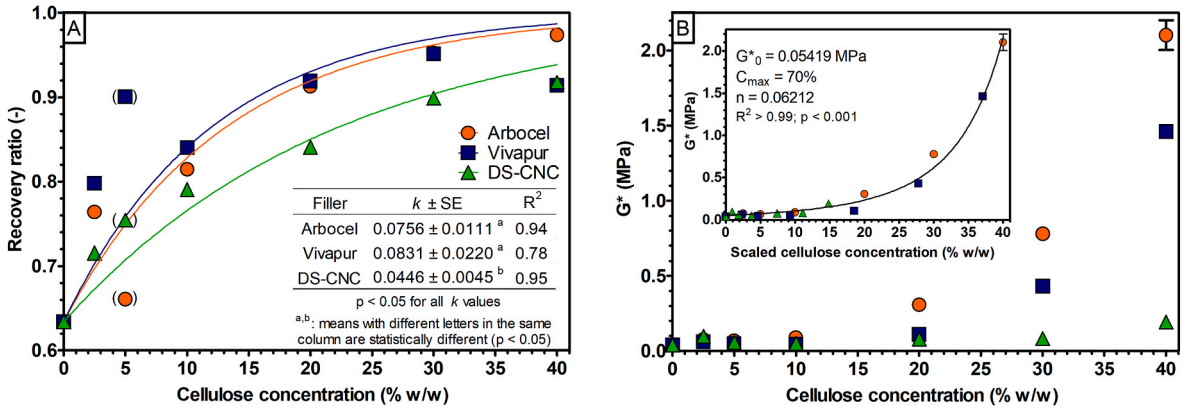

Fig. 7. (A) Recovery ratio calculated using Complex modulus (G*) of composite oleogels from celluloses, Arbocel, Vivapur, and DS-CNC as a function of cellulose concentration. The rate constant (k) from fitting of the one-phase association model (Eq. (2)) is presented in the table as inset. The goodness of fit represented by R^2, standard error of mean (SE), and p indicate the appropriate fitting of the model. With statistical analysis of the estimate (k) (inset in panel A). The data points in panel A in brackets were excluded from regression analysis. (B) G* of the composite oleogels as a function of cellulose concentration. G* was calculated as an average value of initial four points excluding the first two points in the LVR. Inset in panel B: fitting of hyperbolic function to the scaled cellulose concentration.

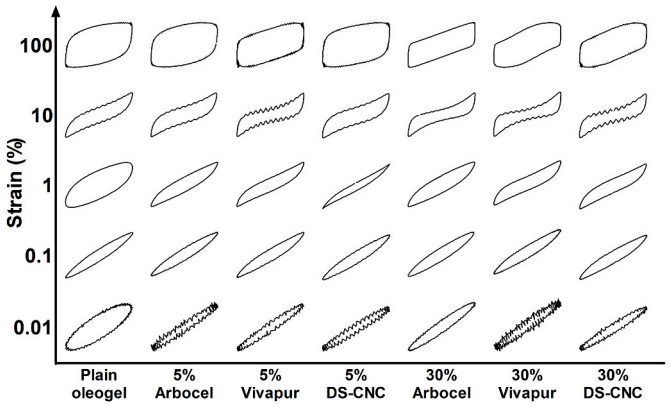

Fig. 8. Compositional Lissajous space of plain oleogel (0% cellulose) and cellulose-filled oleogels at representative compositions. Curves were normalized by their respective maximum stress and maximum strain in each cycle and were acquired at frequency $\omega = 1$ Hz.

composite as the strain increases, as also indicated in the local measures of elasticity and viscosity (Fig. 6, Fig. S5). To ease comparisons among samples, adimensional measures: index of stiffening S and index of thickening T are reported. Expectedly, all samples retain more elasticity at the turnaround point (or large strain) than during flow. This leads to stress upturns within a cycle (or local intracycle strain stiffening as referred to in the literature), as observed in the Lissajous curves (Fig. 8). The general qualitative behavior is very similar for all samples; however, at sufficiently large strain $\gamma = 10\%$, oleogels filled with Arbocel and Vivapur granules display stronger intracycle strain stiffening. This is consistent with the stronger reinforcement in the average moduli G^* (Fig. 6) and the stress response σ (Fig. 7) for Arbocel and Vivapur fillers. Likewise, all composite systems display comparable intracycle strain-rate thinning behavior. This in accordance with the expected behavior of rigid filler particles which perturb the stress and strains set up in the oleogel soft solid, corresponding to increase in elastic energy. Such increase in turn, give increment in the solid elastic constant, leading to stiffening of the composite system. Simultaneously, inclusion of rigid fillers causes composites to become more brittle as $\varphi_{\text{filler}} \rightarrow \varphi_{\text{m}}$, and hence more susceptible to shear-thinning than pure oleogels. Overall, the mechanical properties provided conclusive evidence that cellulose-based fillers act as granular rigid fillers.

Poor resistance of the oleogel network to retain the high amounts of incorporated oil during high-shear conditions largely limits the applications of oleogels. Therefore, the oil-retention ability that was measured during an accelerated oil-release test by centrifuging the samples shows the dependency of concentration and size of cellulose particles. Plain oleogels with a monoglyceride crystal network released approximately 25% oil (Fig. 9). At cellulose weight fraction below 30%, composite oleogels released a higher amount of oil than the plain oleogel regardless of cellulose size (Fig. 9). Above 30% concentration, the effect was cellulose size dependent with microcrystalline celluloses (Arbocel and Vivapur), releasing less oil than DS-CNC and plain oleogel.

It is possible that the addition of filler particles adds fractures or modifies the tortuosity path in the gel-granular medium, easing the oil escape from the matrix at low concentrations (Li, Rombouts, van der Gucht, de Vries, & Dijksman, 2019). With the increasing concentration of cellulose towards the maximum packing fraction in the composite system, the oil escape is decreased due to an increase in tortuosity. The reduced oil release is also attributed to the increase in surface tension above the jamming point due to geometrical constraints that reduce the flowability of the system that transitions from "over-wet" to "dry-like" appearance (Brown & Jaeger, 2014). Crystalline spherulites that were observed in composite oleogels are known to have low structuring ability compared to platelet-like crystals observed in plain oleogels (Patel & Dewettinck, 2016). The lower oil-retention ability of composite oleogels contradicted their strong mechanical properties observed in the

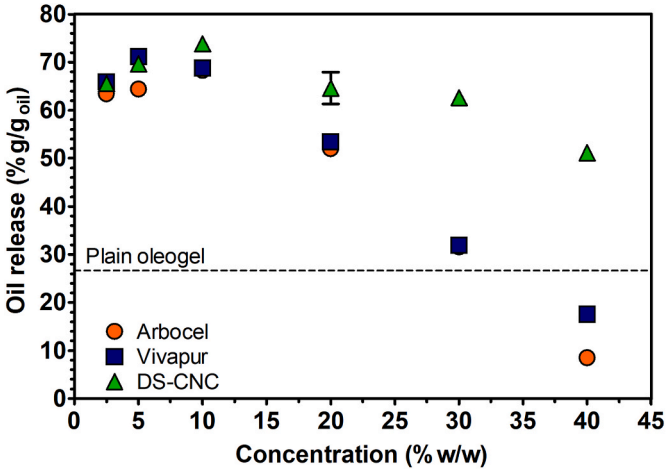

Fig. 9. Oil release over oil weight by composite oleogels from celluloses, Arbocel, Vivapur, and DS-CNC as a function of cellulose concentration compared to plain oleogel.

previous section. It should be noted that for the oil-release test, aliquots of molten oleogels were cooled directly in microtubes and centrifuged to observe the oil release, avoiding sample transfer as in during rheological measurement. Hence the observed oil-release data may be over-estimated and benefit most the plain oleogel.

4. Conclusions

In this study, we demonstrate that crystalline celluloses of different sizes can be used to engineer the structure of oleogels for tunable mechanical properties. The present work demonstrated the size-dependent role of crystalline celluloses in the structural reinforcement of monoglyceride-based oleogels. Cellulose particles were inactive fillers in the composite oleogels and provided a solid substrate for the growing monoglyceride crystals and enabled a better assembly of monoglyceride molecules. This effect was pronounced in oleogels containing microcrystalline cellulose particles. At the microstructural level, the crystal morphology of monoglycerides changed from platelet-like structure to spherulites with no significant changes in the thermal properties of oleogels. Crystalline celluloses improved the mechanical properties and elastic recovery of oleogels, and the effect was size and concentration dependent. The microcrystalline celluloses Arbocel and Vivapur exhibited better structuration abilities than the nanocrystalline cellulose DS-CNC at a given weight fraction in the composite system. We explain the observed effect due to the jammed microstructure of the cellulose particles and monoglyceride crystals, which was evident beyond 30% for microcrystalline celluloses. The observed effect was also applicable in the oil-retention ability of composite oleogels during an accelerated oil-release test. Jammed structures from microcrystalline celluloses beyond 30% released less oil. The work presented here is expected to broaden the practical applications of crystalline cellulose-based composites. Novel functional composite lipid-based materials can be obtained via cellulose micro- and nanocrystals in oleogels that offer better mechanical properties. Such materials can be used in applications such as fat substitutes leading to nutritionally superior food products with increased fiber content.

CRediT authorship contribution statement

Mamata Bhattarai: Conceptualization, Data curation, Formal analysis, Investigation, Methodology, Writing – original draft, Writing – review & editing. **Paavo Penttilä:** Data curation, Formal analysis, Investigation, Writing – review & editing. **Luisa Barba:** Data curation, Formal analysis, Investigation, Writing – review & editing. **Braulio Macias-Rodriguez:** Data curation, Investigation, Writing – review & editing. **Sami Hietala:** Writing – review & editing. **Kirsi S. Mikkonen:** Writing – review & editing. **Fabio Valoppi:** Conceptualization, Data curation, Formal analysis, Resources, Funding acquisition, Investigation, Methodology, Writing – original draft, Writing – review & editing.

Declaration of competing interests

The authors declare that they have no known competing financial interests or personal relationships that could have appeared to influence the work reported in this paper.

The authors declare the following financial interests/personal relationships which may be considered as potential competing interests: Fabio Valoppi reports financial support was provided by Academy of Finland. Fabio Valoppi reports financial support was provided by European Union's Horizon 2020 research and innovation program. Paavo Penttila reports financial support was provided by Academy of Finland. Braulio Macias-Rodriguez reports financial support was provided by European Union's Horizon 2020 research and innovation program. Fabio Valoppi has patent #FI20225150 pending to University of Helsinki. Mamata Bhattarai has patent #FI20225150 pending to University of Helsinki.

Acknowledgments

P.P. and F.V. acknowledge the Academy of Finland (grant numbers P.P.: 315768 and F.V.: 316244). B.M.R. and F.V. acknowledge the European Union's Horizon 2020 research and innovation program funding under grant agreement No. 798917 and No. 836071, respectively. The authors acknowledge facilities and technical support by Nanomicroscopy Center at Aalto University.

Appendix A. Supplementary data

Supplementary data to this article can be found online at https://doi.org/10.1016/j.lwt.2022.113331.

References

Acevedo, N. C., & Marangoni, A. G. (2010). Characterization of the nanoscale in triacylglycerol crystal networks. *Crystal Growth & Design, 10*, 3327–3333. https://doi.org/10.1021/cg100468e

Bergström, M., Pedersen, J. S., Schurtenberger, P., & Egelhaaf, S. U. (1999). Small-angle neutron scattering (sans) study of vesicles and lamellar sheets formed from mixtures of an anionic and a cationic surfactant. *The Journal of Physical Chemistry B, 103*, 9888–9897. https://doi.org/10.1021/jp991846w

Blake, A. I., Co, E. D., & Marangoni, A. G. (2014). Structure and physical properties of plant wax crystal networks and their relationship to oil binding capacity. *Journal of the American Oil Chemists' Society, 91*, 885–903. https://doi.org/10.1007/s11746-014-2435-0

Blake, A. I., & Marangoni, A. G. (2015a). The effect of shear on the microstructure and oil binding capacity of wax crystal networks. *Food Biophysics, 10*, 403–415. https://doi.org/10.1007/s11483-015-9398-z

Blake, A. I., & Marangoni, A. G. (2015b). Plant wax crystals display platelet-like morphology. *Food Structure, 3*, 30–34. https://doi.org/10.1016/j.foostr.2015.01.001

Brown, E., & Jaeger, H. M. (2014). Shear thickening in concentrated suspensions: Phenomenology, mechanisms and relations to jamming. *Reports on Progress in Physics, 77*, Article 046602. https://doi.org/10.1088/0034-4885/77/4/046602

Da Pieve, S., Calligaris, S., Co, E., Nicoli, M. C., & Marangoni, A. G. (2010). Shear nanostructuring of monoglyceride organogels. *Food Biophysics, 5*, 211–217. https://doi.org/10.1007/s11483-010-9162-3

Da Pieve, S., Calligaris, S., Panozzo, A., Arrighetti, G., & Nicoli, M. C. (2011). Effect of monoglyceride organogel structure on cod liver oil stability. *Food Research International, 44*, 2978–2983.

David, A., David, M., Lesniarek, P., Corfias, E., Pululu, Y., Delample, M., et al. (2021). Oleogelation of rapeseed oil with cellulose fibers as an innovative strategy for palm oil substitution in chocolate spreads. *Journal of Food Engineering, 292*, 110315. https://doi.org/10.1016/j.jfoodeng.2020.110315

De France, K. J., Hoare, T., & Cranston, E. D. (2017). Review of hydrogels and aerogels containing nanocellulose. *Chemistry of Materials, 29*, 4609–4631. https://doi.org/10.1021/acs.chemmater.7b00531

Dhal, S., Mohanty, A., Yadav, I., Uvanesh, K., Kulanthaivel, S., Banerjee, I., et al. (2017). Magnetic nanoparticle incorporated oleogel as iontophoretic drug delivery system. *Colloids and Surfaces B: Biointerfaces, 157*, 118–129. https://doi.org/10.1016/j.colsurfb.2017.05.061

Dinkgreve, M., Paredes, J., Denn, M. M., & Bonn, D. (2016). On different ways of measuring "the" yield stress. *Journal of Non-newtonian Fluid Mechanics, 238*, 233–241. https://doi.org/10.1016/j.jnnfm.2016.11.001

Doucet, M., Cho, J. H. A., Gervaise, Attala, Z., Bakker, J., Bouwman, W., et al. (2020). *Sasview version 5.0.3*. Zenodo. https://doi.org/10.5281/zenodo.3930098

Fu, S.-Y., Feng, X.-Q., Lauke, B., & Mai, Y.-W. (2008). Effects of particle size, particle/matrix interface adhesion and particle loading on mechanical properties of particulate–polymer composites. *Composites Part B: Engineering, 39*, 933–961. https://doi.org/10.1016/j.compositesb.2008.01.002

Giacomozzi, A. S., Palla, C. A., Carrín, M. E., & Martini, S. (2019). Physical properties of monoglycerides oleogels modified by concentration, cooling rate, and high-intensity ultrasound. *Journal of Food Science, 84*, 2549–2561. https://doi.org/10.1111/1750-3841.14762

Gravelle, A. J., Blach, C., Weiss, J., Barbut, S., & Marangoni, A. G. (2017). Structure and properties of an ethylcellulose and stearyl alcohol/stearic acid (ec/so:Sa) hybrid oleogelator system. *European Journal of Lipid Science and Technology*, 1700069. https://doi.org/10.1002/ejlt.201700069

Hammersley, A. P., Svensson, S. O., Hanfland, M., Fitch, A. N., & Hausermann, D. (1996). Two-dimensional detector software: From real detector to idealised image or two-theta scan. *High Pressure Research, 14*, 235–248. https://doi.org/10.1080/08957959608201408

Jana, S., & Martini, S. (2014). Effect of high-intensity ultrasound and cooling rate on the crystallization behavior of beeswax in edible oils. *Journal of Agricultural and Food Chemistry, 62*, 10192–10202. https://doi.org/10.1021/jf503393h

Jang, A., Bae, W., Hwang, H. S., Lee, H. G., & Lee, S. (2015). Evaluation of canola oil oleogels with candelilla wax as an alternative to shortening in baked goods. *Food Chemistry, 187*, 525–529. https://doi.org/10.1016/j.foodchem.2015.04.110

Krieger, I. M., & Dougherty, T. J. (1959). A mechanism for non-Newtonian flow in suspensions of rigid spheres. *Transactions of the Society of Rheology, 3*, 137–152. https://doi.org/10.1122/1.548848

Langford, J. I., & Wilson, A. J. C. (1978). Scherrer after sixty years: A survey and some new results in the determination of crystallite size. *Journal of Applied Crystallography, 11*, 102–113. https://doi.org/10.1107/s0021889878012844

Lin, Q., Zhu, X., Fu, Y. P., Zhang, Y. M., Fang, R., Yang, L. Z., et al. (2014). Rationally designed anion-responsive-organogels: Sensing f(-) via reversible color changes in gel-gel states with specific selectivity. *Soft Matter, 10*, 5715–5723. https://doi.org/10.1039/c4sm00841c

Li, X., Rombouts, W., van der Gucht, J., de Vries, R., & Dijksman, J. A. (2019). Mechanics of composite hydrogels approaching phase separation. *PLoS One, 14*, Article e0211059. https://doi.org/10.1371/journal.pone.0211059

Lopez-Martinez, A., Morales-Rueda, J. A., Dibildox-Alvarado, E., Charo-Alonso, M. A., Marangoni, A. G., & Toro-Vazquez, J. F. (2014). Comparing the crystallization and rheological behavior of organogels developed by pure and commercial monoglycerides in vegetable oil. *Food Research International, 64*, 946–957. https://doi.org/10.1016/j.foodres.2014.08.029

Macias-Rodriguez, B. A., Ewoldt, R. H., & Marangoni, A. G. (2018). Nonlinear viscoelasticity of fat crystal networks. *Rheologica Acta, 57*, 251–266. https://doi.org/10.1007/s00397-018-1072-1

Macias-Rodriguez, B. A., & Marangoni, A. A. (2017). Linear and nonlinear rheological behavior of fat crystal networks. *Critical Reviews in Food Science and Nutrition*, 1–18. https://doi.org/10.1080/10408398.2017.1325835

Marangoni, A. G., van Duynhoven, J. P. M., Acevedo, N. C., Nicholson, R. A., & Patel, A. R. (2020). Advances in our understanding of the structure and functionality of edible fats and fat mimetics. *Soft Matter, 16*, 289–306. https://doi.org/10.1039/c9sm01704f

Nikiforidis, C. V., & Scholten, E. (2015). Polymer organogelation with chitin and chitin nanocrystals. *RSC Advances, 5*, 37789–37799. https://doi.org/10.1039/c5ra06451a

Patel, A. R. (2018). Structuring edible oils with hydrocolloids: Where do we stand? *Food Biophysics, 13*, 113–115. https://doi.org/10.1007/s11483-018-9527-6

Patel, A. R., Cludts, N., Bin Sintang, M. D., Lewille, B., Lesaffer, A., & Dewettinck, K. (2014). Polysaccharide-based oleogels prepared with an emulsion-templated approach. *ChemPhysChem, 15*, 3435–3439. https://doi.org/10.1002/cphc.201402473

Patel, A. R., & Dewettinck, K. (2016). Edible oil structuring: An overview and recent updates. *Food & Function, 7*, 20–29. https://doi.org/10.1039/c5fo01006c

Pauw, B. R., Smith, A. J., Snow, T., Terrill, N. J., & Thünemann, A. F. (2017). The modular small-angle x-ray scattering data correction sequence. *Journal of Applied Crystallography, 50*, 1800–1811. https://doi.org/10.1107/S1600576717015096

Peyronel, F., Ilavsky, J., Pink, D. A., & Marangoni, A. G. (2014). Quantification of the physical structure of fats in 20 minutes: Implications for formulation. *Lipid Technology, 26*, 223–226. https://doi.org/10.1002/lite.201400051

Roisnel, T., & Rodríguez-Carvajal, J. (2000). Winplotr: A windows tool for powder diffraction patterns analysis. *Materials Science Forum, 378–381*, 118–123. https://doi.org/10.4028/www.scientific.net/MSF.378-381.118.

Sakai, T., Iijima, K., & Suzuki, K. (2018). Organogel-in-water emulsions as thermal-energy storage and heat transfer fluids. *Journal - Japan Society of Colour Material, 91*, 85–88. https://doi.org/10.4011/shikizai.91.85

Schmidt, P. W. (1991). Small-angle scattering studies of disordered, porous and fractal systems. *Journal of Applied Crystallography, 24*, 414–435. https://doi.org/10.1107/S0021889891003400

Sharifi, M., Goli, S. A. H., & Fayaz, G. (2019). Exploitation of high-intensity ultrasound to modify the structure of olive oil organogel containing propolis wax. *International Journal of Food Science and Technology, 54*, 509–515. https://doi.org/10.1111/ijfs.13965

da Silva, M. A., & Dreiss, C. A. (2016). Soft nanocomposites: Nanoparticles to tune gel properties. *Polymer International, 65*, 268–279. https://doi.org/10.1002/pi.5051

Tanti, R., Barbut, S., & Marangoni, A. G. (2016). Hydroxypropyl methylcellulose and methylcellulose structured oil as a replacement for shortening in sandwich cookie creams. *Food Hydrocolloids, 61*, 329–337. https://doi.org/10.1016/j.foodhyd.2016.05.032

Valoppi, F., Calligaris, S., Barba, L., Šegatin, N., Poklar Ulrih, N., & Nicoli, M. C. (2017). Influence of oil type on formation, structure, thermal, and physical properties of monoglyceride-based organogel. *European Journal of Lipid Science and Technology, 119*, 1500549. https://doi.org/10.1002/ejlt.201500549

Valoppi, F., Calligaris, S., & Marangoni, A. G. (2017). Structure and physical properties of oleogels containing peanut oil and saturated fatty alcohols. *European Journal of Lipid Science and Technology, 119*, 1600252. https://doi.org/10.1002/ejlt.201600252

Valoppi, F., Salmi, A., Ratilainen, M., Barba, L., Puranen, T., Tommiska, O., et al. (2020). Controlling oleogel crystallization using ultrasonic standing waves. *Scientific Reports, 10*, 14448. https://doi.org/10.1038/s41598-020-71177-6

de Vries, A., Hendriks, J., van der Linden, E., & Scholten, E. (2015). Protein oleogels from protein hydrogels via a stepwise solvent exchange route. *Langmuir, 31*, 13850–13859. https://doi.org/10.1021/acs.langmuir.5b03993

Xiao, C., Zhang, Z., Zhang, J., Lu, Y., & Zhang, L. (2003). Properties of regenerated cellulose films plasticized with α-monoglycerides. *Journal of Applied Polymer Science, 89*, 3500–3505. https://doi.org/10.1002/app.12509

Yoshikawa, S., Kida, H., & Sato, K. (2015). Fat crystallization with talc particles is influenced by particle size, concentration, and cooling rate. *European Journal of Lipid Science and Technology, 117*, 858–868. https://doi.org/10.1002/ejlt.201400420